DETC2001/VIB-21363

BASIN OF ATTRACTION OF THE SIMPLEST WALKING MODEL

A. L. Schwab[*]
Laboratory for Engineering Mechanics
Faculty of Mechanical Engineering,
Delft University of Technology,
Mekelweg 2, NL-2628 CD Delft,
The Netherlands
Email: a.l.schwab@wbmt.tudelft.nl

M. Wisse
Delft Biped Laboratory,
Faculty of Mechanical Engineering,
Delft University of Technology,
Mekelweg 2, NL-2628 CD Delft,
The Netherlands
Email: m.wisse@wbmt.tudelft.nl

KEYWORDS

Multibody dynamics; passive dynamic walking; walking robots; bipeds; ballistic walking; basin of attraction.

ABSTRACT

Passive dynamic walking is an important development for walking robots, supplying natural, energy-efficient motions. In practice, the cyclic gait of passive dynamic prototypes appears to be stable, only for small disturbances. Therefore, in this paper we research the basin of attraction of the cyclic walking motion for the simplest walking model. Furthermore, we present a general method for deriving the equations of motion and impact equations for the analysis of multibody systems, as in walking models. Application of the cell mapping method shows the basin of attraction to be a small, thin area. It is shown that the basin of attraction is not directly related to the stability of the cyclic motion.

1   INTRODUCTION

The past few decades robotics research has made huge developments in the area of biped locomotion, running from prosthesis development to entertainment industries. Several major institutes have succeeded in building successful walking bipeds. One of the under-addressed problems is energy consumption. Most existing bipeds need an 'umbilical cord' for power supply.

Honda Motor Co. (Hirai *et al.*, 1998) developed a completely autonomous humanoid robot, but it has to carry 20 kilograms of batteries for a 15 minute walk.

A solution for energetic efficiency is the exploitation of the 'natural dynamics' of the locomotive system. McGeer introduced the idea of 'passive dynamic walking' (McGeer, 1990a), inspired by research of Mochon and McMahon (Mochon and McMahon, 1980). They showed that in human locomotion the motion of the swing leg is merely a result of gravity acting on an unactuated double pendulum. McGeer extended the idea and showed that a completely unactuated and therefore *uncontrolled* robot can perform a stable walk (McGeer, 1989).

The walking motion of a passive dynamic walker is started by launching the robot with such initial values for the leg angles and velocities, that the end of that step (the beginning of a new step) is nearly identical to the starting conditions. A periodic or cyclic walking motion will then result. At each step, when the heel strikes the floor, the impact will result in loss of energy. This loss can be compensated for by having the robot walk down a shallow slope or by periodically supplying energy with an actuator.

A recent study by Garcia, Chatterjee, Ruina, and Coleman (Garcia *et al.*, 1998) showed that the simplest passive dynamic walking model can have stable cyclic motion. Experience with real prototypes however reveals that even a very small disturbance may result in failure. This leads us to believe that the size of allowable disturbances is at least as important as the stability

---

[*]Address all correspondence to this author.

of the cyclic solution. Therefore, in this paper we will investigate the basin of attraction of the cyclic motion and the failure modes for the simplest walking model.

2 THE SIMPLEST WALKING MODEL

The subject of this research is the simplest mechanical model still possessing the ability to perform a bipedal walking motion, as conceived by Garcia *et al.* (Garcia *et al.*, 1998). The model, shown in Figure 1, consists of two rigid links with length l, connected by a frictionless hinge at the hip. The mass is distributed over three point masses; one with mass M at the hip, and two with mass m at the feet. The limit case where the foot mass is negligible in comparison with the hip mass, $\beta = m/M \rightarrow 0$, is investigated. This unactuated two-link system walks down a slope in a gravity force field with magnitude g. The scaled model of the walker with unit M, l, and g, now only has one free parameter, the slope angle γ.

A walking step is started with both feet on the slope. The front foot has just made ground contact, the hind foot has a velocity away from the floor. During a step, the stance foot is modeled as a hinge, connected to the floor. The swing foot is moving freely as the other end of a double pendulum. At about midstance, the swing foot will briefly be below floor level ('footscuffing'), which is inevitable for a walker with straight legs. Knees (McGeer, 1990b; Wisse and Schwab, 2001; Adolfsson *et al.*, 2001; Collins *et al.*, 2001) or other leg shortening measures (Van der Linde, 1998), as well as 3D motion (Kuo, 1999; Van der Linde, 1998; Van der Linde, 1999) would solve the problem but increase complexity of the model. After this short through-pass, the second time that the swing foot reaches floor level is regarded as heel-strike, the end of the step. The former swing foot makes a fully inelastic collision and becomes the new stance leg. Instantaneously, the former stance leg looses ground contact, and a new step begins.

3 ANALYSIS OF THE MODEL

In the analysis of the passive dynamic walking motion, three stages can be distinguished. First, the derivation of the equations of motion for the walker during the support phase. They will be derived in terms of independent coordinates by the principle of virtual power and will be solved by numeric integration. Second, we formulate and apply the impact equations governing the heelstrike. Third and last, we will formulate the support exchange and combine the results from the previous stages in a stride function. The 'stride function' (McGeer, 1992) is a Poincaré map relating the state during one part of a step with the state during the same part of the next step.
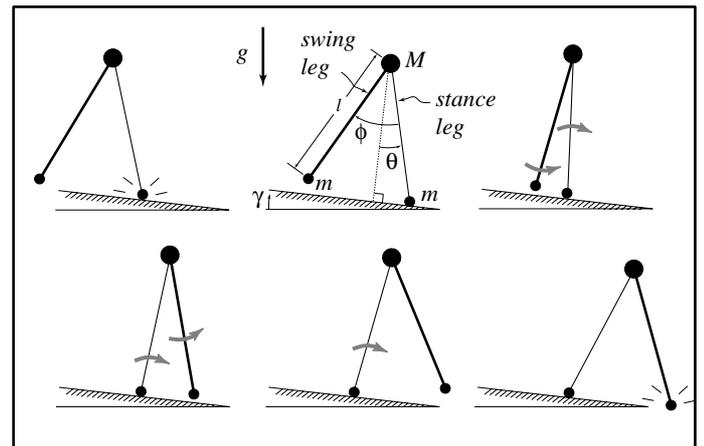

Figure 1. A typical passive walking step. The new stance leg (lighter line) has just made contact with the ramp in the upper left picture. The swing leg (heavier line) swings until the next heelstrike (bottom right picture). The top-center picture gives a description of the variables and parameters that we use. θ is the angle of the stance leg with respect to the slope normal. ϕ is the angle between the stance leg and the swing leg. M is the hip mass, and m is the foot mass. l is the leg length. γ is the ramp slope, and g is the acceleration due to gravity. Reprinted with permission from Garcia *et al.* (Garcia *et al.*, 1998)

3.1 Equations of Motion

The configuration of the walker is defined by the coordinates of the three point masses; the stance foot, the hip and the swing foot, which can be arranged in a global vector $\mathbf{x} = (x_{stl}, y_{stl}, x_{hip}, y_{hip}, x_{swl}, y_{swl})^T$. These coordinates are not independent owing to the two distance constraints imposed by the stance and the swing leg. In order to eliminate the constraint forces from the start, we shall express the equations of motion in terms of independent generalized coordinates. Let Oxy be a fixed orthogonal system of coordinates with Ox along the walking slope and Oy directed upward. Then u and v are the coordinates of the contact point of the stance foot. During walking motion they will be fixed, but at heel-strike they will have no boundary condition in order to fulfill the "lifting stance foot" assumption. Furthermore, θ is the angle between the stance leg and Oy, and ϕ the clockwise angle between the stance leg and the swing leg. The configuration of the walker can be described by the vector of generalized coordinates $\mathbf{q} = (u, v, \theta, \phi)^T$. The coordinates $\mathbf{x}$ can locally be expressed as functions of the generalized coordinates $\mathbf{q}$, the kinematic degrees of freedom (configuration

coordinates), by means of a transfer function $\mathbf{F}$ as

$$\mathbf{x} = \mathbf{F}(\mathbf{q}) \rightarrow \begin{bmatrix} x_{stl} \\ y_{stl} \\ x_{hip} \\ y_{hip} \\ x_{swl} \\ y_{swl} \end{bmatrix} = \begin{bmatrix} u \\ v \\ u - \sin(\theta) \\ v + \cos(\theta) \\ u - \sin(\theta) + \sin(\theta - \phi) \\ v + \cos(\theta) - \cos(\theta - \phi) \end{bmatrix}. \quad (1)$$

The unreduced equations of motion for the system are obtained by assembling the contribution to the virtual power equation of all point masses in a global mass matrix $\mathbf{M}$ and a global force vector $\mathbf{f}$, which results in a virtual power balance

$$\delta\dot{\mathbf{x}}^T[\mathbf{f} - \mathbf{M}\ddot{\mathbf{x}}] = 0. \quad (2)$$

Here, $\delta\dot{\mathbf{x}}$ are kinematically admissible virtual velocities, which satisfy all instantaneous kinematic constraints. By differentiating the transfer function (1) we obtain

$$\dot{\mathbf{x}} = \mathbf{F}_{,\mathbf{q}}\dot{\mathbf{q}}, \quad \delta\dot{\mathbf{x}} = \mathbf{F}_{,\mathbf{q}}\delta\dot{\mathbf{q}} \quad \text{and} \quad \ddot{\mathbf{x}} = \mathbf{F}_{,\mathbf{q}}\ddot{\mathbf{q}} + \mathbf{F}_{,\mathbf{q}\mathbf{q}}\dot{\mathbf{q}}\dot{\mathbf{q}}. \quad (3)$$

Here a subscript comma followed by one or more variables denotes partial derivatives with respect to these variables. The way in which higher-order derivatives have to be multiplied by the juxtaposed vectors goes without saying. Substitution of these expressions in the virtual power equation (2) and adding on the left-hand side the contribution, $\delta\dot{\mathbf{q}}^T\mathbf{Q}$, from the generalized forces $\mathbf{Q}$ dual to the coordinates $\mathbf{q}$, yields the reduced equations of motion

$$[\mathbf{F}_{,\mathbf{q}}^T\mathbf{M}\mathbf{F}_{,\mathbf{q}}]\ddot{\mathbf{q}} = \mathbf{F}_{,\mathbf{q}}^T[\mathbf{f} - \mathbf{M}\mathbf{F}_{,\mathbf{q}\mathbf{q}}\dot{\mathbf{q}}\dot{\mathbf{q}}] + \mathbf{Q}. \quad (4)$$

For the walker the global mass matrix is

$$\mathbf{M} = \mathrm{Diag}(\beta, \beta, 1, 1, \beta, \beta), \quad (5)$$

and the applied forces, only gravity, are

$$\mathbf{f} = \mathbf{M}[\sin(\gamma), -\cos(\gamma), \sin(\gamma), -\cos(\gamma), \sin(\gamma), -\cos(\gamma)]^T, \quad (6)$$

and zero for the generalized forces Q_θ and Q_ϕ. The contact condition on the stance foot gives the boundary conditions $u = 0$ and $v = 0$. This contact is only valid for compressive vertical contact force, $Q_v > 0$, and will be checked during the simulation. After solving the unknown accelerations of the generalized coordinates

$\ddot{\mathbf{q}}$ from the reduced equations of motion (4) and then taking the limit yields

$$\lim_{\beta \to 0} \ddot{\mathbf{q}} = \begin{bmatrix} \ddot{\theta} \\ \ddot{\phi} \end{bmatrix} = \begin{bmatrix} \sin(\theta - \gamma) \\ \sin(\phi)(\dot{\theta}^2 - \cos(\theta - \gamma)) + \sin(\theta - \gamma) \end{bmatrix}, \quad (7)$$

and for the unknown contact forces

$$\lim_{\beta \to 0} \begin{bmatrix} Q_u \\ Q_v \end{bmatrix} = \begin{bmatrix} \sin(\theta)(\dot{\theta}^2 - \cos(\theta - \gamma)) \\ -\cos(\theta)(\dot{\theta}^2 - \cos(\theta - \gamma)) \end{bmatrix}. \quad (8)$$

In the case of a more complicated walker, as for example in the 3D passive dynamic biped with yaw and roll compensation (Wisse and Schwab, 2001), it will be impractical to solve symbolically for the accelerations of generalized coordinates. A numerical evaluation of every individual contribution to the reduced equations of motion (4) and its solution is more practical. A limit case can be handled by a small order perturbation.

3.2 Heelstrike

We assume that the heel strike behaves as a fully inelastic impact (no slip, no bounce), which is in accordance with observations on existing passive dynamic walking prototypes. Also, double stance is assumed to occur instantaneously. As soon as the swing foot hits the floor the stance foot lifts up, not interacting with the ground during impact. The resulting vertical velocity of the lifting foot should then be pointed upwards. If this is confirmed after the impact equations are solved, the assumption is verified. Otherwise, the walker would come to a complete stop. Treating heel strike as an impact, we assume that velocities change instantaneously. These velocity jumps are enforced by very high values of the contact forces acting only during a small time interval of contact. In the limit case the first go to infinity and the second goes to zero. The integral of the force with respect to time over the duration of the impact, the impulse, has a finite value which is the cause of the velocity jump. While the impact takes place all positions as well as all non-impulsive forces of the system remain constant. The impact is usually divided into a compression and an expansion phase. Newton's impact law links these two phases by stating that the relative speed after impact equals e times the relative speed before impact but in opposite direction. The factor e is the coefficient of restitution. A value of $e = 1$ corresponds with a fully elastic impact whereas the value of $e = 0$ represents a completely inelastic impact in which the two parts "stick" together after impact. The reduced equations of motion (4) written in terms of the generalized coordinates $\mathbf{q}$ are

$$\bar{\mathbf{M}}\ddot{\mathbf{q}} = \bar{\mathbf{f}}, \quad (9)$$

3

with the reduced mass matrix and force vector

$$\bar{\mathbf{M}} = [\mathbf{F}_{,\mathbf{q}}^T \mathbf{M} \mathbf{F}_{,\mathbf{q}}], \quad \bar{\mathbf{f}} = \mathbf{F}_{,\mathbf{q}}^T [\mathbf{f} - \mathbf{M} \mathbf{F}_{,\mathbf{qq}} \dot{\mathbf{q}} \dot{\mathbf{q}}] + \mathbf{Q}. \quad (10)$$

Note that the "lifting stance foot"-assumption implies that the system has no boundary conditions on the former stance foot and consequently there are more degrees of freedom during impact than during smooth motion. The uni-lateral constraints at heel strike are expressed by the contact functions $\mathbf{g}$, the coordinates of the swing foot expressed in terms of the generalized coordinates as

$$\mathbf{g}(\mathbf{q}) = \begin{bmatrix} g_x \\ g_y \end{bmatrix} = \begin{bmatrix} x_{swl} \\ y_{swl} \end{bmatrix} = \begin{bmatrix} u - \sin(\theta) + \sin(\theta - \phi) \\ v + \cos(\theta) - \cos(\theta - \phi) \end{bmatrix}. \quad (11)$$

When contact occurs, detected by a change of sign in the swing foot vertical clearance function g_y, the former swing foot becomes constrained in both the x and y direction and the equations of motion become

$$\bar{\mathbf{M}} \ddot{\mathbf{q}} + \mathbf{g}_{,\mathbf{q}}^T \boldsymbol{\lambda} = \bar{\mathbf{f}}, \quad (12)$$

with the Lagrangian multipliers $\boldsymbol{\lambda}$ dual to the relative contact velocities $\dot{\mathbf{g}}$. These multipliers can be interpreted as the contact forces. Integration of these equations of motion over the time of impact and taking the limit case yields

$$\lim_{t^- \uparrow t^+} \int_{t^-}^{t^+} (\bar{\mathbf{M}} \ddot{\mathbf{q}} + \mathbf{g}_{,\mathbf{q}}^T \boldsymbol{\lambda}) dt = 0. \quad (13)$$

The reduced force vector $\bar{\mathbf{f}}$ only contains non-impulsive forces and therefore the right-hand side vanishes. Under the introduction of the contact impulses,

$$\boldsymbol{\rho} = \lim_{t^- \uparrow t^+} \int_{t^-}^{t^+} \boldsymbol{\lambda} \, dt, \quad (14)$$

and noting that the mass matrix, in general a function of the generalized coordinates, remains constant during impact, the momentum equations for the system become

$$\bar{\mathbf{M}} \dot{\mathbf{q}}^+ + \mathbf{g}_{,\mathbf{q}}^T \boldsymbol{\rho} = \bar{\mathbf{M}} \dot{\mathbf{q}}^- \quad (15)$$

with $\dot{\mathbf{q}}^-$ the velocities before and $\dot{\mathbf{q}}^+$ the velocities of the system after impact. Together with Newton's impact law,

$$\dot{\mathbf{g}}^+ = -e \dot{\mathbf{g}}^-, \quad \text{or} \quad \mathbf{g}_{,\mathbf{q}} \dot{\mathbf{q}}^+ = -e \mathbf{g}_{,\mathbf{q}} \dot{\mathbf{q}}^-, \quad (16)$$

we have a complete set of linear equations reading

$$\begin{bmatrix} \bar{\mathbf{M}} & \mathbf{g}_{,\mathbf{q}}^T \\ \mathbf{g}_{,\mathbf{q}} & 0 \end{bmatrix} \begin{bmatrix} \dot{\mathbf{q}}^+ \\ \boldsymbol{\rho} \end{bmatrix} = \begin{bmatrix} \bar{\mathbf{M}} \dot{\mathbf{q}}^- \\ -e \mathbf{g}_{,\mathbf{q}} \dot{\mathbf{q}}^- \end{bmatrix} \quad (17)$$

From these equations the velocities after impact $\dot{\mathbf{q}}^+$ together with the contact impulses $\boldsymbol{\rho}$ can be found. Because Newton's impact law (16) is often contradicted experimentally in case of multiple impacts, a restriction to simple impacts is made. The contact configuration for the walker is denoted by $u = 0$, $v =$ constant, and $\phi = 2\theta$. The velocities of the stance foot before impact are zero. Solving the impact equations at the contact configuration and subsequently taking the limit case yields for the velocities after impact

$$\lim_{\beta \to 0} \dot{\mathbf{q}}^+ = \begin{bmatrix} \dot{u}^+ \\ \dot{v}^+ \\ \dot{\theta}^+ \\ \dot{\phi}^+ \end{bmatrix} = \begin{bmatrix} -\sin(\theta)\cos(2\theta)\sin(2\theta) \\ \cos(\theta)\cos(2\theta)\sin(2\theta) \\ \cos^2(2\theta) \\ \cos(2\theta)(\cos(2\theta) - 1) \end{bmatrix} \dot{\theta}^-, \quad (18)$$

and for the contact impulses

$$\lim_{\beta \to 0} \boldsymbol{\rho} = \begin{bmatrix} \rho_x \\ \rho_y \end{bmatrix} = \begin{bmatrix} -\sin(\theta)\sin(2\theta) \\ \cos(\theta)\sin(2\theta) \end{bmatrix} \dot{\theta}^-. \quad (19)$$

The limit case, with the only moving mass in the hip, gives us some easy to verify results. First, the velocities after impact are only a function of the stance leg angle θ and its angular velocity $\dot{\theta}^-$. This velocity is in fact the hip velocity. Second, the contact impulse at the heel strike is directed along the swing leg with magnitude $\sin(2\theta)\dot{\theta}^-$, which is the projection of the hip velocity just before impact on the swing leg. And last, the stance foot velocity after impact is $\cos(2\theta)\sin(2\theta)\dot{\theta}^-$ in the direction of the stance leg, this is the hip velocity after impact projected on this leg.

3.3 Stride function
The mapping from the initial conditions $\mathbf{v} = (\mathbf{q}, \dot{\mathbf{q}})$, from one step to the next is the so-called 'stride function' (McGeer, 1992), reading

$$\mathbf{v}_{n+1} = \mathbf{S}(\mathbf{v}_n). \quad (20)$$

If we start the walker with the initial conditions on the state as $(\theta, \phi, \dot{\theta}, \dot{\phi})_0$, then after the first heelstrike (18) two initial conditions drop out and the next state is only dependent on θ and $\dot{\theta}^-$. In this paper we look for a motion of the walker were the two legs pivot and swing, no full turns, and return to the same state

4

after one heelstrike, the so called period-one gait cycle. For the analysis of the gait we have to swap the stance and swing leg variables from step n to step $n+1$ as

$$\begin{aligned} \theta_{n+1} &= \theta_n - \phi_n \\ \phi_{n+1} &= -\phi_n. \end{aligned} \quad (21)$$

At heelstrike, the swing leg angle ϕ^- is equal to $2\theta^-$, and combining the time derivatives of (21) with the velocities after impact (18), gives us the initial conditions after heelstrike as

$$\begin{aligned} \theta_{n+1} &= -\theta_n^- \\ \phi_{n+1} &= -2\theta_n^- \\ \dot\theta_{n+1} &= \cos(2\theta^-)\dot\theta_n^- \\ \dot\phi_{n+1} &= \cos(2\theta^-)(1-\cos(2\theta^-))\dot\theta_n^-. \end{aligned} \quad (22)$$

The stride function for the simplest walker is now; starting with $(\theta_n, \dot\theta_n)$ as the initial conditions at the beginning of the nth step, numerically integrating the equations of motion (4) until heelstrike occurs, then calculating the velocities after heelstrike and finally swapping the legs (22), resulting the initial conditions $(\theta_{n+1}, \dot\theta_{n+1})$ of the next step.

4 STEP-TO-STEP BEHAVIOR

For a large range of initial conditions at step n, the stride function has no result; the model does not make a complete walking step so that there cannot be a subsequent step. Usually, the stride function has one or two cyclic solutions: initial conditions that map onto themselves. If a cyclic solution is stable, there exists a region surrounding it, which asymptotically leads to this solution. This region is called the basin of attraction. We will determine this basin of attraction by the cell mapping method.

4.1 Failure modes

We limited the searching area for practical reasons by exclusion of uninteresting and unfeasible initial conditions. First, as mentioned in Section 3.3, after the first heelstrike there are only two independent initial conditions, θ and $\dot\theta$. This reduces the Poincaré section to a 2D area. Second, only forward walking is investigated, so $\theta > 0$ and $\dot\theta < 0$. And last, from (22) it is clear that after heelstrike, $\dot\theta_{n+1}$ can only be negative (forward motion) if $\theta < \frac{\pi}{4}$ [rad]. Within this area, the general behavior is classified in Figure 2. Exemplary motion of the walker is at a slope $\gamma = 0.004$ [rad]. The area of possible initial conditions is roughly bisected by the line $\dot\theta_0 = -\theta_0 + \gamma$. Above this line, the input energy (initial velocity) is not enough to overcome the 'dead point' (compare this with an inverted pendulum), and the walker falls Backwards. Below this line, the walker falls Forwards. This occurs when the swing foot does not rise above floor level, after the

short through-pass at midstance. In between these areas, a small region exists in which a walking step can occur. Some of these steps lead to failure (F or B) after a sequence of steps, while others will lead to perpetual walking, the small basin of Attraction. At large angles and high speeds, walking is not possible. In the model, a tensile vertical foot contact force occurs, $Q_v < 0$. Real walking mechanisms would lose foot contact and with both feet in the air we classify this as Running. Note that this is more or less equal to the commonly used boundary of Froude number $v^2/(gl) > 1$.
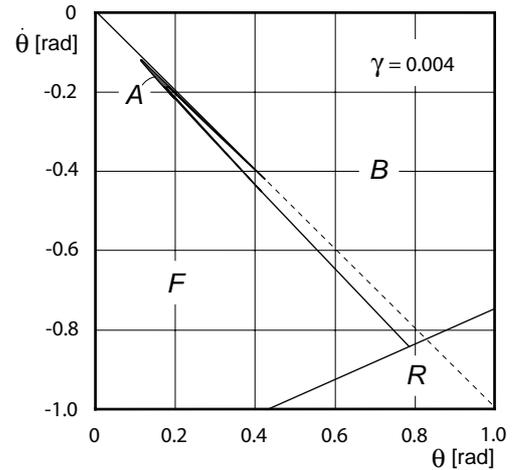
Figure 2. Poincaré section for the simplest walker with initial stance leg angle θ and velocity $\dot\theta$ together with failure modes; falling Forwards, falling Backwards and Running, and the basin of Attraction of the cyclic walking motion $(\theta, \dot\theta) = (0.1534, -0.1561)$ [rad] at a slope of $\gamma = 0.004$ [rad].

4.2 Cyclic motion

If the model is started inside the basin of attraction, it settles eventually into a repetitive motion, the attractor. The walker is in cyclic motion if the stride pattern repeats itself after a fixed number of strides. Looking at the Poincaré map of the state of the system at the beginning of each step we recognize this cyclic motion as a fixed point. The method for finding cyclic gait, as commonly used in passive dynamic walking research, is as follows. A walking cycle is specified by the requirement that the vector of initial conditions $\mathbf{v}_n$ results in identical initial conditions for the kth subsequent step:

$$\mathbf{v}_{n+k} = \mathbf{v}_n \quad (23)$$

5

A vector with initial conditions satisfying this requirement is a cyclic solution $\mathbf{v}_c$, which maps onto itself:

$$\mathbf{S}^k(\mathbf{v}_c) = \mathbf{v}_c \tag{24}$$

The main interest is symmetric walking, or $k = 1$. Such cyclic solution can be found by a linearization of the stride function

$$\begin{aligned} \mathbf{S}(\mathbf{v} + \Delta\mathbf{v}) &\approx \mathbf{S}(\mathbf{v}) + \mathbf{J}\Delta\mathbf{v} \\ \text{with} \quad \mathbf{J} &= \frac{\partial \mathbf{S}}{\partial \mathbf{v}} \end{aligned} \tag{25}$$

and applying a Newton-Raphson iteration procedure, starting with a set of initial conditions $\mathbf{v}$ close to the cyclic solution $\mathbf{v}_c$

$$\begin{aligned} &\text{repeat} \\ &\quad \Delta\mathbf{v} = [\mathbf{I} - \mathbf{J}]^{-1}(\mathbf{S}(\mathbf{v}) - \mathbf{v}) \\ &\quad \mathbf{v} = \mathbf{v} + \Delta\mathbf{v} \\ &\text{until } |\Delta\mathbf{v}| < \varepsilon \end{aligned} \tag{26}$$

where $\mathbf{I}$ is the identity matrix. The Jacobian $\mathbf{J}$ is calculated by a perturbation method, which involves simulation of a full walking step for every initial condition. The eigenvalues of $\mathbf{J}$ quantify the stability of the cyclic motion. If both eigenvalues are inside the unit circle in the complex plane, a basin of attraction exists, with at least the size of the perturbation used to calculate the Jacobian. From Garcia, it is known that the simplest walking model has a stable cyclic walking motion for slopes up to 0.015 [rad], see Figure 3.
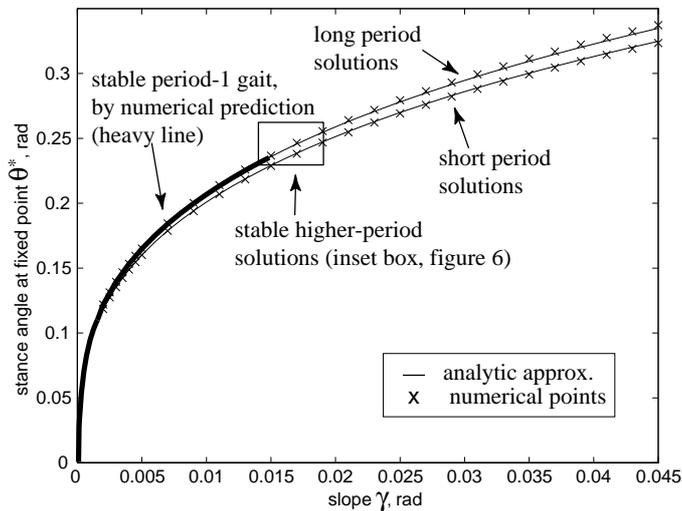
4.3 Cell mapping method

The general behavior of the stride function can be studied with the aid of the cell mapping method (Hsu, 1987). The region of feasible initial conditions is subdivided into a large number (N) of small cells. All unfeasible initial conditions are regarded as a small number (z) of very large cells, so called *sink cells*. The cells are numbered 1 to N+z. By application of the stride function to the centre of each cell, all of the N+z cells point to initial conditions inside one of the other cells, except the sink cells which point to themselves by definition. Starting with cell 1, a sequence of cells appears by following the pointers. This sequence either ends in a sink cell or in a repetitive cycle. This cycle can consist of one self-repeating cell (a fixed point, which could be a sink cell), or a number of cells (comparable to multiple-period walking, Garcia (Garcia *et al.*, 1998)). The repetitive cycle is identified and all cells in the sequence are labeled as basin of attraction of that cycle. Then the procedure is repeated with all N cells. As soon as a known cell (from a previous sequence) is encountered, the procedure can be stopped, and all cells in that sequence are labeled as basin of attraction of that last cell.

Application of the cell mapping method results in a list with all attractors (cyclic solutions) and classification of all discretization points into this list. Not only period-one walking gaits can be found, also period-k walking gaits. Results of the cell mapping method are as accurate as the discretization, within these tolerances fixed points may come and go. For example, what appears to be a fixed cell might in fact be slowly changing initial conditions (smaller changes than the discretization) of subsequent steps.

Figure 3. Stance leg angle θ at fixed point versus slope angle γ. Reprinted with permission from Garcia *et al.* (Garcia *et al.*, 1998).

5   RESULTS

All initial conditions leading to perpetual walking are contained inside the basin of attraction, which for the simplest walker is roughly speaking a small, pointy boomerang. If started inside the basin of attraction, the initial conditions of a sequence of steps spiral towards the self-repeating cyclic solution. The size and shape of the basin of attraction diminish at increasing slope angle. Above a certain slope angle, the basin of attraction completely disappears and no stable cyclic solutions exist.

5.1   Basin of Attraction

From Figure 2 it is obvious that the basin of attraction is only a very small region. For better insight in the shape, Figure 2 is zoomed in and sheared, leading to Figure 4. The vertical axis now represents the sum of the stance leg angle and scaled angular velocity. The horizontal line at $\theta + \dot{\theta} = 0$ corresponds with the '-45 degree'-line in Figure 2. Figure 4 is obtained with application of the cell mapping method with a discretization of about 200×250 points ($\Delta\theta = 0.002$ [rad], $\Delta(\theta + \dot{\theta}) = 0.0002$ [rad]), the drawn lines are a manual continuous interpretation of the discrete boundary of the basin of attraction.
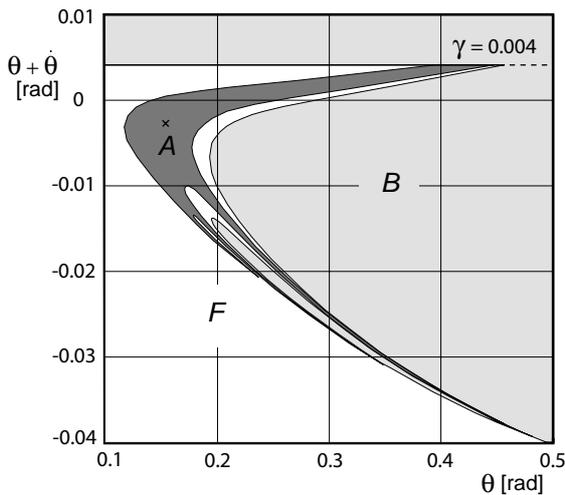

Figure 4.   Poincaré section for the simplest walker, enlarged and sheared section from Figure 2, together with failure modes; falling <u>F</u>orwards, falling <u>B</u>ackwards, and the basin of <u>A</u>ttraction of the cyclic walking motion.

Figure 4 shows that the small basin of attraction is mostly bounded by falling backward on one side and falling forward on the other side. The basin of attraction seems to be a continuous and tailing area. The different areas show fractal-like entanglement. We will discuss the behavior of the walker in these areas by going over a vertical line, $\theta = 0.2$ [rad], in Figure 4 from area F to area B, crossing the basin of attraction at least four times. Point

($\theta = 0.2$ [rad], $\dot{\theta} = -0.23$ [rad]) lies in area F. If started with such initial conditions, the walking model will fall forwards; the swing leg is allowed to pass through the floor to ignore the otherwise inevitable foot-scuffing, but does not rise above floor level anymore. Going up, the area changes from falling <u>F</u>orwards to the basin of <u>A</u>ttraction. Just before crossing this boundary, the behavior changes. Not the first step after these initial conditions is failing, but the model first walks some steps before eventually falling forwards. The closer to the basin of attraction, the more steps it takes before failure. If started in the first tail of the basin of attraction, encountered when going up, the walker will eventually settle into steady cyclic walking with initial conditions of the fixed point. The path towards the fixed point is presented in Figure 5 and in table 1. The motion of the legs is shown in Figure 6. After nine steps, the walker is close to the fixed point, and continuing the simulation will show asymptotic approach.

step	θ [rad]	$\dot{\theta}$ [rad]	$\theta + \dot{\theta}$ [rad]
1	0.2000	-0.2165	-0.01645
2	0.1788	-0.1917	-0.01290
3	0.1756	-0.1841	-0.00850
4	0.1878	-0.1888	-0.00100
5	0.1586	-0.1599	-0.00134
6	0.1459	-0.1488	-0.00295
7	0.1492	-0.1526	-0.00337
8	0.1539	-0.1569	-0.00302
9	0.1558	-0.1583	-0.00256
$\vdots$	$\vdots$	$\vdots$	$\vdots$
f.p.	0.1534	-0.1561	-0.00269

Table 1.   Initial conditions of a number of subsequent steps, started just inside the basin of attraction and going to the fixed point.

Even more up on the line ($\theta = 0.2$), area F is encountered again. Starting there leads to falling forward after a number of steps. In this manner, A, B, and F are crossed several times, until we reach $\theta + \dot{\theta} = \gamma$. Above this boundary, the stance leg will not reach midstance and fall backwards. In general, if started inside the basin of attraction, the initial conditions spiral towards the fixed point. If started just outside the basin of attraction, the walker will take a few steps but eventually fail. The further away, the smaller the amount of successful steps before failure.
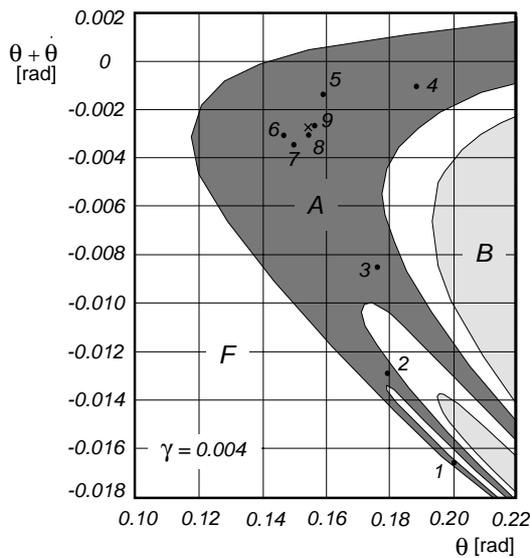
Figure 5. A number of steps, started just inside the basin of attraction and going to the fixed point. Together with failure modes; falling Forwards, falling Backwards, and the basin of Attraction of the cyclic walking motion.
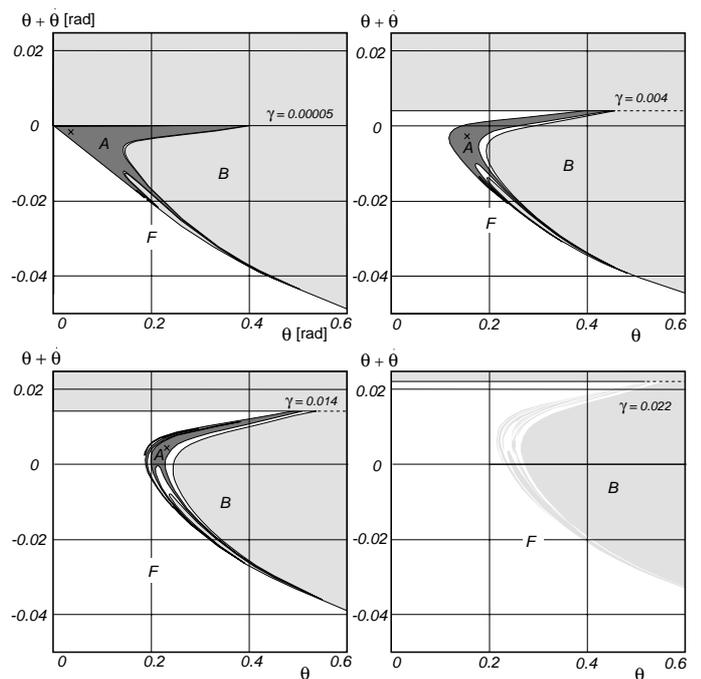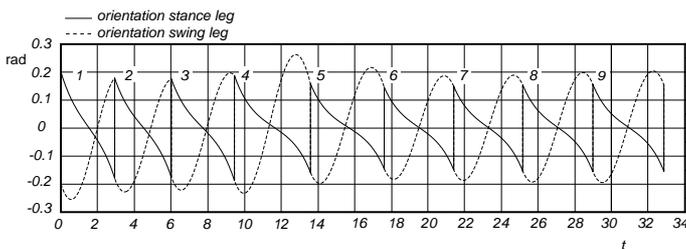

Figure 6. Orientation of the stance leg, solid line, and swing leg, dotted line, with respect to the normal on the slope for a walker started just inside the basin of attraction and going to the fixed point.

5.2 Basin of attraction versus slope angle

The size of the basin of attraction determines the amount of disturbance that the walker can handle without falling. The stability of the fixed point determines if, and how fast the walker recovers from a small disturbance. The latter analysis is less time-consuming and therefore very useful to determine the existence of a basin of attraction. The applicability of the walker however depends on the allowable size of disturbances. Therefore, we investigate the dependency of the basin of attraction on the only model parameter, the ramp slope γ. Figure 7 shows the development of the basin of attraction for an increasing ramp slope γ. As the slope increases, the basin of attraction decreases in size and gets more and more tails at the boundaries, which appears to be fractal-like. At and beyond a slope angle of 0.022 [rad] the basin of attraction has vanished.

Figure 7. Development of the basin of attraction with increasing floor slopes, together with failure modes; falling Forwards, falling Backwards, and the basin of Attraction of the cyclic walking motion.

We compare the size of the basin of attraction with the stability of the cyclic motion, see Figure 8. The stability is measured as the largest of the two eigenvalues (modulus) of the linearized stride function (25). As stated by Garcia *et al.* (Garcia *et al.*, 1998), for $0 < \gamma < 0.0151$ [rad] the period-one gait is stable. For higher slopes, only higher-period gaits are stable, having a small basin of attraction. The eigenvalues would lead to believe that a slope $\gamma = 0.012$ [rad] would be preferable. However, the basin of attraction, measured as the number of cells inside the basion of attraction times the area of one cell, is not at its maximum. Clearly, there is no direct relation between the stability of the cyclic motion and its basin of attraction.

6 CONCLUSIONS

The basin of attraction of the simplest walking model is very small. This explains why physical models only walk successfully if started carefully on a very flat and rigid surface. The basin of attraction is surrounded by a region of initial conditions that lead to successful walking for a limited number of steps, eventually resulting in failure. The simplest walker has two failure modes; falling forward and falling backward. We expect to find qualitatively similar failure behavior in more complex walkers, although these would have more failure modes.

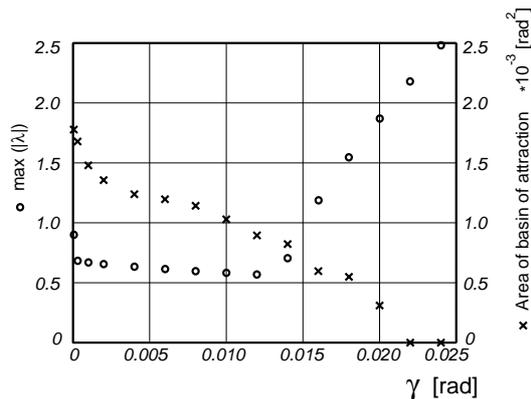Our research shows that there is no obvious relation between

8

Figure 8. The stability of the cyclic motion and the area of the basin of attraction versus slope angle γ.

the size of the basin of attraction and the stability of the fixed point. Therefore, the most robust design would probably not be the one with the best linearized stability, but the one with the largest basin of attraction. It is our intention to continue this research and find in which manner various passive and active measures on the walker can increase the basin of attraction.

ACKNOWLEDGEMENTS

REFERENCES

Hirai, K., Hirose, M., Haikawa, Y., and Takenaka, T., 1998, "The development of honda humanoid robot," *Proceedings of the IEEE International Conference on Robotics and Automation*, Piscataway, NJ, pp. 1321–1326.

McGeer, T., 1990a, "Passive dynamic walking," International Journal of Robotics Research, **9**(2), pp. 62–82.

Mochon, S., and McMahon, T. A., 1980, "Ballistic walking," Journal of Biomechanics, **13**, pp. 49–57.

McGeer, T., 1989, "Powered flight, child's play, silly wheels, and walking machines," *Proceedings of the IEEE International Conference on Robotics and Automation*, Piscataway, NJ, pp. 1592–1597.

Garcia, M., Chatterjee, A., Ruina, A., and Coleman, M. J., 1998, "The simplest walking model: Stability, complexity, and scaling," ASME Journal of Biomechanical Engineering, **120**(2), pp. 281–288.

McGeer, T., 1990b, "Passive walking with knees," *Proceedings of the IEEE International Conference on Robotics and Automation*, Los Alamitos, CA, pp. 1640–1645.

Wisse, M., and Schwab, A.L., 2001, "A 3d passive dynamic biped with roll and yaw compensation," To appear in Robotica.

Adolfsson, J., Dankowicz, H., and Nordmark, A., 2001, "3d passive walkers: finding periodic gaits in the presence of discontinuities," Nonlinear Dynamics, **24**(2), pp. 205-229.

Collins, S. H., Ruina, A., Wisse, M., and Coleman, M. J., 2001, "A two legged kneed passive dynamic walking robot," In preparation for the International Journal of Robotics Research.

Van der Linde, R. Q., 1998, "Active leg compliance for passive walking," *Proceedings of the IEEE International Conference on Robotics and Automation*, Piscataway, NJ, pp. 2339–2344.

Kuo, A. D., 1999, "Stabilization of lateral motion in passive dynamic walking," International Journal of Robotics Research, **18**(9), pp. 917–930.

Van der Linde, R. Q., 1999, "Passive bipedal walking with phasic muscle contraction," Biological Cybernetics, **81**(3), pp. 227–237.

McGeer, T., 1992, "Passive dynamic biped catalogue," in Chatila, R., and Hirzinger, G. (eds.), *Proceedings Experimental Robotics II: The 2nd International Symposium*, Springer–Verlag, Berlin, pp. 465–490.

Hsu, C. S., 1987, *Cell–to–cell mapping; a method of global analysis for nonlinear systems*, Applied mathematical sciences 64, Springer, New York.